# Photonic corner skin modes in non-Hermitian photonic crystals

Weiwei Zhu [1,2,3,4] and Jiangbin Gong [2,5,6,*]

[1]*College of Physics and Optoelectronic Engineering, Ocean University of China, Qingdao 266100, China*
[2]*Department of Physics, National University of Singapore, Singapore 117551*
[3]*Engineering Research Center of Advanced Marine Physical Instruments and Equipment of Education Ministry, Ocean University of China, Qingdao 266100, China*
[4]*Qingdao Key Laboratory for Optics Photoelectronics, Ocean University of China, Qingdao 266100, China*
[5]*Centre for Quantum Technologies, National University of Singapore, Singapore 117543*
[6]*Joint School of National University of Singapore and Tianjin University, International Campus of Tianjin University, Binhai New City, Fuzhou 350207, China*

(Received 28 February 2023; revised 19 June 2023; accepted 27 June 2023; published 12 July 2023)

Useful in the enhancement of light-matter interaction, localization of light is at the heart of photonics studies. Different approaches have been proposed to localize light, including those based on dynamical localization, topological trivial or nontrivial defects in the band gap of photonic crystals, and bound states in the continuum. Recent studies on the non-Hermitian skin effect have provided us new means to localize waves. Inspired by two recent studies [Li *et al.*, Phys. Rev. Lett. **128**, 223903 (2022); Zhu and Gong, Phys. Rev. B **106**, 035425 (2022)], we propose an innovative method towards localized light in continuous systems via photonic corner skin modes, which are hybrid skin-topological modes as a special kind of second-order non-Hermitian skin effect with symmetrically distributed gain and loss. Specifically, we propose to make use of weak pseudoinversion symmetric gain and loss, which does not close the band gap of the system, to realize a non-Hermitian photonic Chern insulator with chiral edge states. The chiral edge states then accumulate at certain corners of the system. Intriguing phenomena such as corner skin modes arising from an underlying bipolar second-order non-Hermitian skin effect and multiple-corner skin modes are predicted in continuous systems.

DOI: 10.1103/PhysRevB.108.035406

## I. INTRODUCTION

Due to the non-Hermitian skin effect (NHSE), the spectrum of a non-Hermitian system is sensitive to its boundary condition. Under open boundary conditions (OBCs), NHSE in one-dimensional systems causes all the bulk states to localize at one edge of the system [1–4]. While the NHSE itself has topological origin associated with point-gap topology [3–5], it also challenged our understanding of the usual bulk-boundary correspondence in topological band theory and even led to the concept of generalized bulk-boundary correspondence, via which the topological invariants are defined in the so-called generalized Brillouin zone [6–10].

To date, the first-order NHSE has been widely studied both in theory and experiment [1–3,4,6–11]. However, there are much less studies on the second-order NHSE, where certain states (the number of states is proportional to the length of the system) are localized at the corner, with the bulk states still extended [12–25]. Some studies proposed to design second-order NHSE from the Benalcazar-Bernevig-Hughes model [14,17]. This design requires positive couplings along one direction and negative couplings along the opposite direction; clearly exotic features not easy to be realized in experiment. Okugawa *et al.* studied second-order NHSE by connecting it with an intrinsic or extrinsic second-order topological insulator [15]. The models used therein are also yet to be realized in experiments. Hybrid skin-topological modes representing a second type of second-order NHSE are more accessible to experiments, but still requiring specially designed asymmetric couplings, hence limiting its possible extensions [12,13,19,23]. Another kind of hybrid skin-topological modes without asymmetric couplings has been proposed recently, which are realized by adding gain/loss to Chern insulators or anomalous Floquet topological insulators [24,25]. This new development provides us one way to realize a special kind of second-order NHSE without asymmetric couplings. However, it was only discussed in tight-binding models while the Chern insulator is more accessible in continuous models, such as the gyromagnetic photonic crystal. To further explore second-order NHSE for possible applications, we shall explore in this work possible hybrid skin-topological modes (as second-order NHSE) in continuous systems, specifically in photonic crystals.

Photonic crystals, whose material parameters and geometric structure can be easily tuned, have already been proven to be a good platform to study different topological states [26–34]. Actually the classical wave analogy of a Chern insulator was first proposed and realized in gyromagnetic photonic crystals [35–37]. The Floquet topological insulator and Weyl semimetal were all first realized in photonic crystals even earlier than their electric counterparts [38,39]. More importantly, photonic crystals are also a good platform to study non-Hermitian physics where the loss is ubiquitous from material absorption or mode leaking and the gain can be obtained from electrical or optical pumping

*phygj@nus.edu.sg

 

[40,41]. There are also great efforts to study non-Hermitian photonic topological states, mainly in one-dimensional systems [42–52]. Though non-Hermitian Chern bands have been studied in lattice models [53–56], there is less work on non-Hermitian photonic Chern insulators using two-dimensional photonic crystals [57–59]. Our study here shall stimulate further interest in non-Hermitian Chern insulator phases in two-dimensional photonic crystals as continuous systems.

Studies of topological states and non-Hermitian physics in photonic crystals may be relevant to a wide variety of applications, such as topological delay line, high sensitivity sensors, and topological lasers [60–65]. Indeed, topological defects as one way to localize light has attracted much attention for the possibility to enhance light-matter interactions [66–69]. NHSE as a new way to localize light has also been studied in photonic crystals most recently [70–77]. However, the second-order version of NHSE featured in this work as photonic corner skin modes is still not investigated in continuous systems.

In this paper, we propose one way to obtain photonic corner skin modes by adding pseudoinversion symmetric gain/loss to gyromagnetic photonic crystals, which supports chiral edge states. Different from previous studies on hybrid skin-topological modes in lattice models [24,25], this work establishes one simple way to realize hybrid skin-topological modes in continuous systems. Indeed, the spectrum of the edge states is complex under mixed boundary condition and real under OBC. This sensitivity to the boundary conditions constitutes a clear feature of hybrid skin-topological modes. Correspondingly, the eigenfield is extended along the edge under mixed boundary condition and localized at the corner under OBC. We also found a new phenomenon called bipolar second-order NHSE. Similar to the bipolar NHSE from twisted spectral winding numbers in one-dimensional systems [78–81], we observe that part of the chiral edge states are localized at one corner and others are localized at the opposite corner. This is so even though the spectrum of the edge states does not form a loop due to a quantum anomaly [35]. Such intriguing phenomena exist in both square lattices and triangular lattices with pseudoinversion symmetry. Furthermore, by constructing a unit cell preserving pseudo sixfold rotation symmetry, it is found that the corner skin modes can be simultaneously localized at multiple corners in a triangular lattice. In addition, the position of localization of the corner modes is found to depend on frequency in the continuous systems we study.

This work is organized as follows. In Sec. II, we review the Hermitian gyromagnetic photonic crystal, which supports topological chiral edge states in both square lattices and triangular lattices. In Sec. III, we first provide a general understanding of the formation of corner skin modes by accumulation of chiral edge states with gain and loss. Then we discuss the concrete behavior of corner skin modes in various lattices with different designs of gain/loss. Section IV concludes this work. All the simulations are performed in COMSOL MULTIPHYSICS and we only consider the transverse-magnetic modes. We use the sign convention of the rf modulo in COMSOL, where the positive (negative) imaginary parts represent loss (gain).

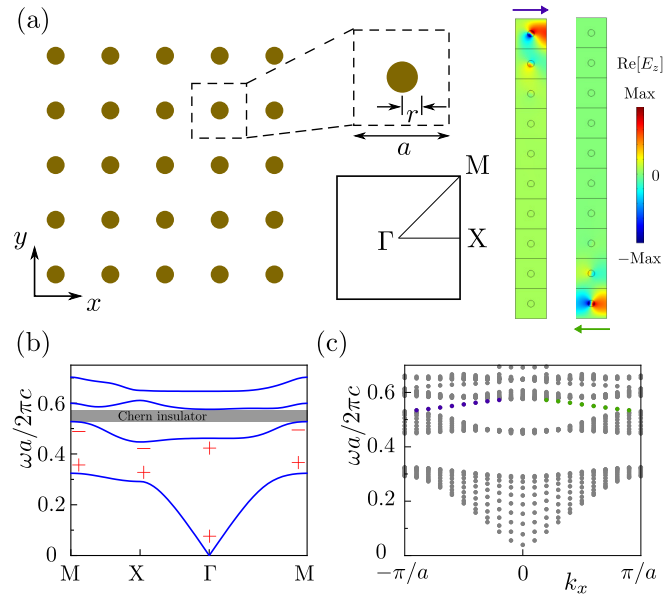


FIG. 1. Topological chiral edge state of gyromagnetic photonic crystal in a square lattice. (a) Two-dimensional photonic crystal in a square lattice is composed of gyromagnetic rods of radius $0.11a$, with $a$ being the lattice constant. The background is air. The unit cell and first BZ are shown at right. (b) The bulk bands along the high symmetric line in first BZ. The parity symmetries at high symmetric momentum points are marked for the lower two bands. $+$ $(-)$ indicates even (odd) parity of the eigenstates. The second band gap is a Chern insulator. (c) The projected band structure as a function of $k_x$. In calculation, periodic boundary condition (PBC) is used along $x$ and OBC is used along $y$. OBC is realized by setting the boundary as perfect electric conductors. The second band gap supports chiral edge states, one (purple) propagating to the right at the upper boundary and the other one (green) propagating to the left at the lower boundary.

## II. TOPOLOGICAL CHIRAL EDGE STATES IN PHOTONIC CRYSTALS WITHOUT NON-HERMITICITY

We first introduce the gyromagnetic photonic crystals, which have been used to realize reflection-free topological edge states [36,82–84]. One example is shown in Fig. 1(a), where the rods made of gyromagnetic materials are regularly distributed in a square lattice and the background is air. The parameters are the same as in Ref. [36] with the lattice constant being $a$, the radius of the rods being $r = 0.11a$, and the relative permittivity of the rods being $\epsilon_r = 15$. The time-reversal symmetry is broken by magnetic field along the $z$ direction and the corresponding relative permeability is a tensor

$$\mu_r = \begin{pmatrix} 14 & 12.4i & 0 \\ -12.4i & 14 & 0 \\ 0 & 0 & 1 \end{pmatrix}. \tag{1}$$

From the unit cell in Fig. 1(a), one can see that the system preserves fourfold rotation symmetry, which contains the inversion symmetry with $\epsilon_r(\mathbf{r}) = \epsilon_r(-\mathbf{r})$ and $\mu_r(\mathbf{r}) = \mu_r(-\mathbf{r})$. The first Brillouin zone is plotted in Fig. 1(a). $\Gamma$, $X$ and $M$ are the high symmetric momentum points.

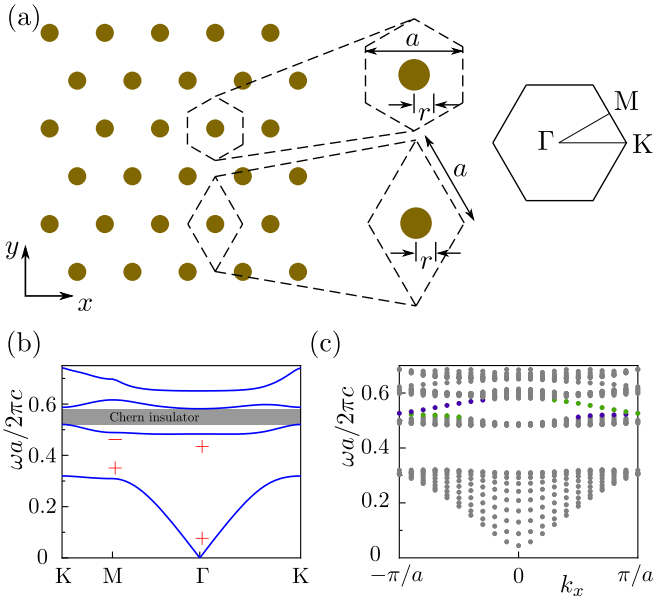


FIG. 2. Same as in Fig. 1, except for triangular photonic crystal. (a) Structure of the photonic crystal in a triangular lattice. (b) The bulk bands along a high symmetric line. (c) The projected band structures.

The bulk band structure along the high symmetric line in the first Brillouin zone is studied and shown in Fig. 1(b). Usually, the topological properties of the bulk band can be described by the Chern number defined from the Bloch states over the whole Brillouin zone [36,85]. Here we quickly check the topological properties by considering the inversion symmetry eigenvalues at inversion symmetric momentum points. From Fig. 1(b), it is seen that the inversion symmetry eigenvalues are all positive for the first band and possesses an odd number of positive eigenvalues for the second band. This indicates that the second band gap has a nonzero Chern number (the Chern number of a band gap is the sum of Chern numbers of all bulk bands below the band gap). Such results are confirmed by the projected band structure shown in Fig. 1(c), where the right-propagating chiral edge states (purple) are localized at the upper edge and the left-propagating chiral edge states (green) are localized at the lower edge.

We carry out a parallel study with the same system parameters but in a triangular lattice as shown in Fig. 2(a). The unit cell can be chosen as hexagon, which preserves sixfold rotation symmetry, or rhombus, which preserves inversion symmetry. Different from the squarelattice case, the high symmetric momentum points for the triangular lattice are Γ, $M$, and $K$. In addition, only Γ and $M$ are inversion symmetry invariant momentum points. The bulk band structure is shown in Fig. 2(b), which is quite similar to the square lattice case because the triangular lattice can be obtained by a slight geometric transformation from the square lattice. Just like the square lattice case, the inversion symmetry eigenvalues are all positive for the first band and possesses an odd number of positive eigenvalues for the second band, indicating again that the second band gap has a nonzero Chern number. Indeed, the chiral edge states can be observed in the second band gap of projected band structure as shown in Fig. 2(c).

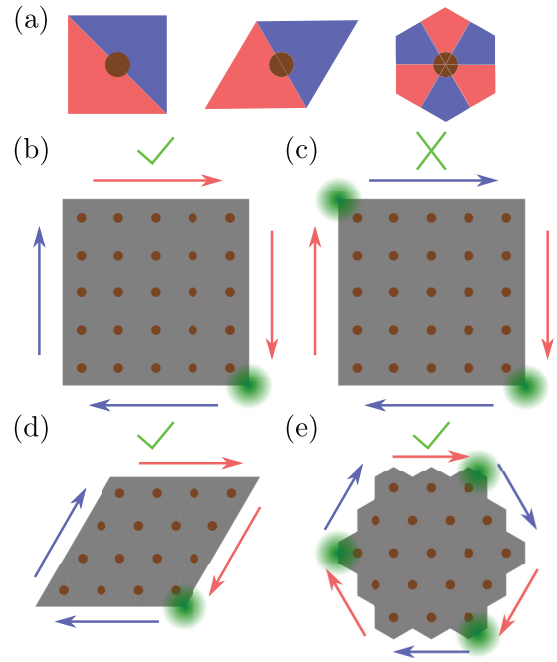


FIG. 3. Schematic for corner skin modes in non-Hermitian photonic crystals with pseudoinversion symmetry. (a) Three examples of the unit cell with pseudoinversion symmetry. The red (blue) part indicates gain (loss). (b) One possible configuration for the chiral edge states localized at one corner. (c) One pseudoinversion symmetry forbidden configuration where the chiral edge states are localized at two corners. (d),(e) Two possible configurations for the chiral edge states localized at one or three corners.

Because the right-propagating edge states and the left-propagating edge states are spatially separated (they are orthogonal to each other), we can describe the topological edge states shown in Figs. 1(c) and 2(c) by a diagonal Hamiltonian under the basis of the upper edge state and the lower edge state $(\psi_{\text{up}}, \psi_{\text{down}})^T$. The Hamiltonian of the edge states can be described by

$$H_{\text{edge}} = \omega_r \sigma_0 + v(k_x - k_r)\sigma_z. \tag{2}$$

Here $\omega_r$ is a reference angular frequency in the middle of the second band gap, $k_r$ is a reference momentum, and $v$ is the group velocity. $v > 0$ in our system, meaning that the upper (lower) edge state propagates to the right (left). $\sigma_0$ is the two-by-two identity matrix and $\sigma_z$ is the third Pauli matrix. This Hamiltonian of the edge states is useful for the understanding of photonic corner skin modes later.

## III. PHOTONIC CORNER SKIN MODES IN NON-HERMITIAN PHOTONIC CRYSTALS WITH PSEUDOINVERSION SYMMETRY

### A. General understanding of photonic corner skin modes

The photonic Chern insulators are quite robust even when the system has non-Hermiticity. With non-Hermiticity, the topological chiral edge states are still there without the band gap closing [53–58]. We introduce gain and loss to the unit cell as illustrated by some examples in Fig. 3(a), where the red area represents gain and the blue area represents loss.

The unit cell still preserves pseudoinversion symmetry with $\epsilon_r(\mathbf{r}) = \epsilon_r^\dagger(-\mathbf{r})$ and $\mu_r(\mathbf{r}) = \mu_r^\dagger(-\mathbf{r})$. As a general analysis, note that if the chiral edge states contain gain (loss) in the upper edge, then we can conclude that the chiral edge states in the lower edge contain loss (gain) due to the pseudoinversion symmetry. The Hamiltonian of the edge states is then modified as

$$H^m_{\text{edge}} = \omega_r \sigma_0 + v(k_x - k_r)\sigma_z + i\gamma\sigma_z. \tag{3}$$

The gain and loss can be treated as a modification to the quasimomentum $\tilde{k}_x = k_x + i\gamma/v$, which makes the waves localize to the right (left) for $\gamma < 0$ ($\gamma > 0$) due to NHSE under OBC. Different from the usual NHSE in a one-dimensional (1D) chain, here the spectrum of the edge state does not form a loop so that it cannot be described by spectral winding numbers but by the sign of $\gamma$.

The localization of chiral edge states can be understood from a general picture. Figures 3(b)–3(e) show some configurations of the chiral edge states with gain/loss. The red (blue) arrow represents gain (loss) chiral edge states. Gain (loss) chiral edge states accumulate waves to (opposite to) the propagation direction. Figure 3(b) is one possible configuration for the square lattice where the waves are localized at the right-down corner due the accumulation effect. Figure 3(c) shows the configuration where the waves are localized at two opposite corners. However, the chiral edge states on the opposite edge having the same gain/loss are forbidden by the pseudoinversion symmetry. So for the square lattice case, all the waves are localized at one corner. For the triangular lattice case, however, it is possible to localize the eigenstate at one corner or three corners as shown in Figs. 3(d) and 3(e).

### B. Photonic corner skin modes due to bipolar second-order NHSE

We now study non-Hermitian photonic crystals in a square lattice with pseudoinversion symmetry, whose unit cell is shown in the inset figure of Fig. 4(a). The gain (loss) is added to the air by tuning the relative permittivity to $\epsilon_r = 1 - 0.8i$ ($\epsilon_r = 1 + 0.8i$). The spectrum of the system with PBC in both dimensions is investigated and shown in Fig. 4(a). The eigenstates are classified into two clusters corresponding to the second bulk band and the third bulk band. There is a line band gap between two bulk bands. Here the terminology "line band gap" is based on the definition in Ref. [5], where a non-Hermitian Hamiltonian is defined to have a line band gap if and only if its complex-energy bands do not cross a reference line in the complex-energy plane. We then study the spectrum of mixed boundary condition and the results are shown in Fig. 4(b). It shows that the bulk band clusters become tighter than that in PBC. The reason is that the nonreciprocal bulk band combined with the gain and loss enables the system to support first-order NHSE, so that the bulk spectrum is sensitive to the boundary condition [73]. In addition, there are complex chiral edge states across the line band gap. The spectrum for the system with OBC in both directions is shown in Fig. 4(c). Again the bulk spectrum becomes tighter. More importantly, the spectrum of chiral edge states has a dramatic change from complex under the mixed boundary condition to real under OBC. Such dramatic change of the spectrum

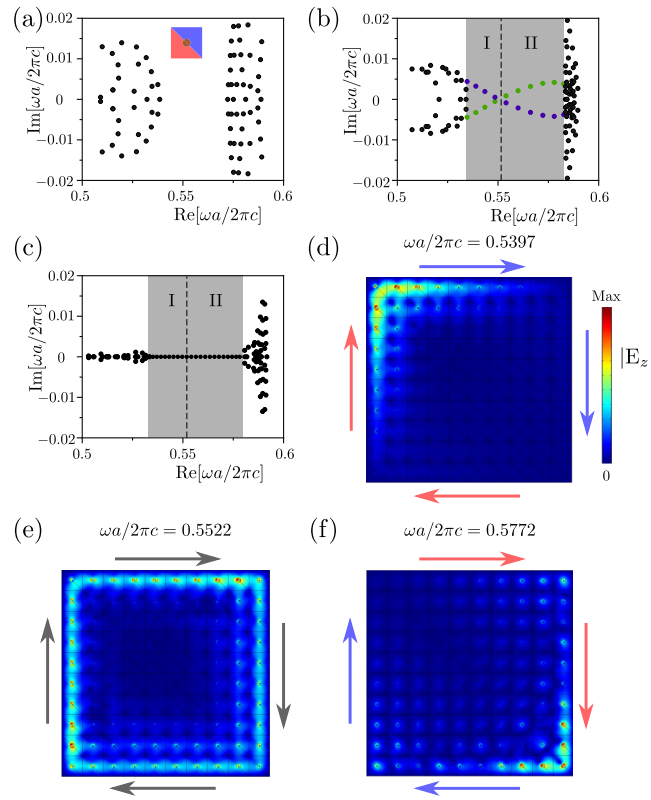


FIG. 4. Corner skin modes in square lattice with pseudoinversion symmetry. (a) Spectrum for the system with PBC in both directions. Unit cell is shown in the inset. (b) Spectrum of the system with mixed boundary condition: PBC in one direction and OBC in another direction. The edge states for the upper (lower) boundary are purple (green). (c) Spectrum for the system with OBC in both directions. (d)–(f) The field profiles for the topological edge states in open boundary condition. (d) Corner skin modes with lower energy are localized at the left-up corner, (e) extended topological edge states at the transition point, and (f) corner skin modes with higher energy is localized at the right-down corner.

is one feature of NHSE. Specifically, we witness NHSE in topological edge states and the essence of physics here can hence be understood as second-order NHSE.

We now focus on the spectrum of edge states in the second band gap. Under the mixed boundary condition, the spectrum of the edge states can be split into two parts as shown in Fig. 4(b): in the first part marked by I, the up (down) edge state has loss (gain) corresponding to $\gamma > 0$ and in second part marked by II, the up (down) edge state has gain (loss) corresponding to $\gamma < 0$. According to Eq. (3), these two parts have different localization behavior in OBC. The eigenfields with OBC are shown in Figs. 4(d)–4(f). It is seen that for part I the waves are localized at the left-up corner shown in Fig. 4(d), at the transition point the waves are extended along the edge shown in Fig. 4(e), and for part II the waves are localized at the right-down corner shown in Fig. 4(f). These phenomena are clearly the two-dimensional counterpart of the so-called bipolar NHSE observed in 1D systems (roughly speaking, bipolar NHSE can localize waves at two opposite directions). For completeness, we note that bipolar NHSE is

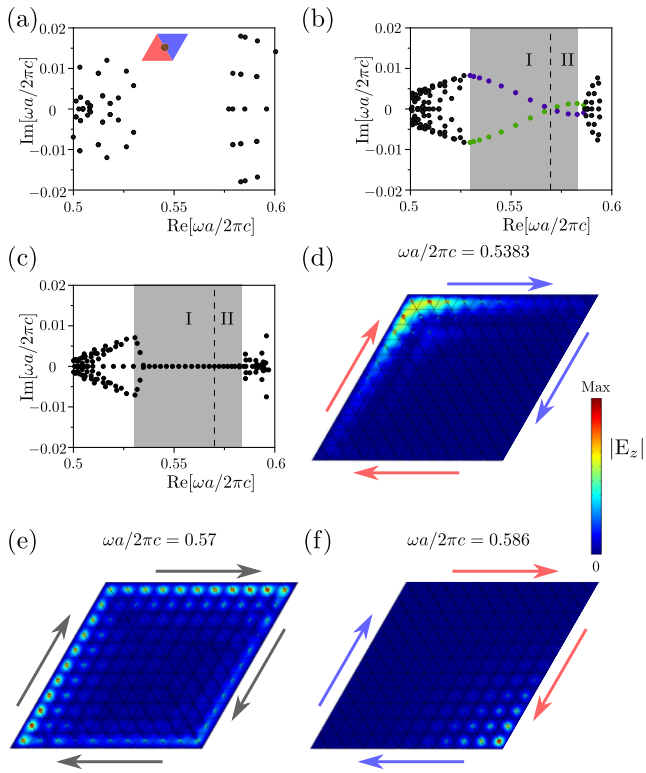


FIG. 5. Same as in Fig. 4, except for triangular photonic crystal. (a) The spectrum for the system with PBC in both directions. (b) The spectrum for the system with mixed boundary condition. (c) The spectrum for the system with OBC in both directions. (d)–(f) The field profiles are shown to illustrate the transition between different localization behavior of corner modes.

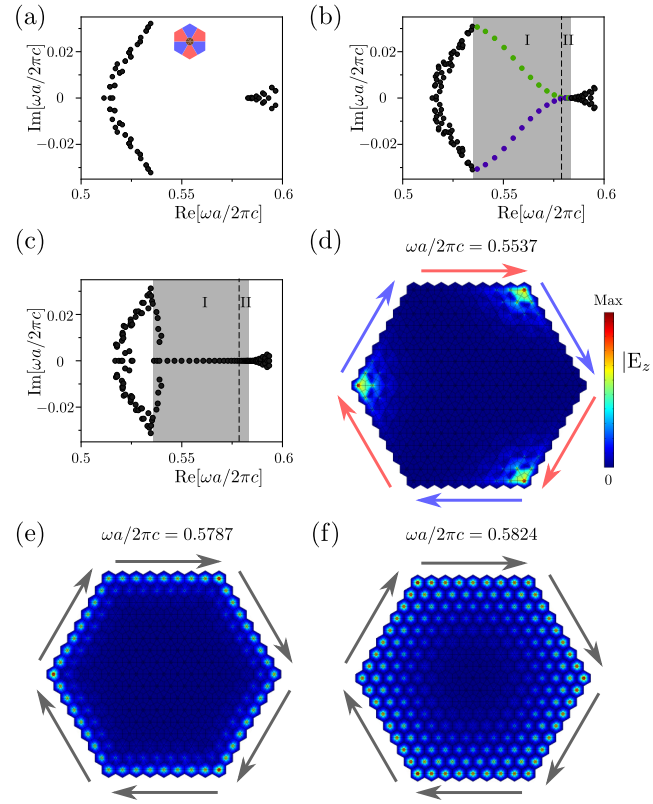


FIG. 6. Corner skin modes in a triangular lattice configuration with pseudo $C_6$ symmetry. (a) The spectrum of the system with PBC in both directions. (b) The spectrum of the system with mixed boundary condition. (c) The spectrum for the system with OBC in both directions. (d) The field profiles for one-corner skin modes where the fields are localized at three corners. (e),(f) Two examples of extended topological edge states.

usually connected with a twisted spectral winding [78–81], and here the so-called twisted spectral winding produces two oppositely oriented loops in contact rather than a single loop [see Figs. 4(b) and 5(b)]. Arising from the interplay of long-range and short-range couplings, the observation of bipolar NHSE usually needs specially designed couplings [78–81]. Interestingly, in the photonic crystal model we study here, the long-range couplings are naturally there and thus make it easy to realize bipolar NHSE. Because the corner modes discussed here are always of second order, the bipolar localization phenomena here can be understood as bipolar second-order NHSE.

Next we examine a similar photonic crystal but in a triangular lattice configuration. The unit cell is shown in the inset figure of Fig. 5(a). Similar phenomena have been observed. Compared with the square lattice case, the bulk spectrum is less sensitive to the boundary conditions as shown in Figs. 5(a)–5(c). The spectrum of the edge states is, however, still sensitive to the boundary conditions, which are complex in mixed boundary condition and real in OBC as shown in Figs. 5(b) and 5(c). There are also two parts: part I corresponding to $\gamma > 0$ and part II corresponding to $\gamma < 0$. In part I, the waves are localized at the left-up corner as shown in Fig. 5(d), at phase transition point the waves are extended along the edge as shown in Fig. 5(e), and in part II the waves are localized at the right-down corner as shown in Fig. 5(f).

### C. Multiple-corner skin modes

Above we have shown that the photonic corner skin modes are localized at one corner. Next we provide a case where the photonic corner skin modes are localized at multiple corners. The unit cell under consideration is shown in the inset figure of Fig. 6(a). The unit cell preserves pseudo sixfold rotation symmetry with $\epsilon_r(\mathbf{r}) = \epsilon_r^\dagger(C_6\mathbf{r})$ and $\mu_r(\mathbf{r}) = \mu_r^\dagger(C_6\mathbf{r})$, which includes the pseudoinversion symmetry with $\epsilon_r(\mathbf{r}) = \epsilon_r^\dagger(-\mathbf{r})$ and $\mu_r(\mathbf{r}) = \mu_r^\dagger(-\mathbf{r})$. The spectrum for the system with PBC in both directions is shown in Fig. 6(a). As in the previous case, there are two bulk band clusters. The spectrum for the system with mixed boundary condition and OBC in both directions are shown in Figs. 6(b) and 6(c). Obviously, the bulk spectrum is almost unchanged in different boundary conditions. The edge spectrum is again quite sensitive to the boundary condition insofar as the edge spectrum is complex under mixed boundary condition and real under OBC. Focusing on the spectrum of the edge states, we again see that they still can be split into two parts: part I and part II. Under mixed boundary condition, the spectrum of edge states is complex in part I corresponding to $\gamma > 0$ and real in part II corresponding to $\gamma = 0$. According to the analysis below Eq. (3), the waves are localized in part I and extended in part II when we choose OBC in both directions. Such results are confirmed by the field

profiles. For states belonging to part I, the waves are localized at three corners as shown in Fig. 6(d). For part II, the waves are extended as shown in Figs. 6(e) and 6(f).

## IV. CONCLUSION AND DISCUSSION

Motivated by earlier findings of hybrid skin-topological modes without asymmetric couplings using lattice models, here we have extended the concept to continuous systems and presented an innovative way to localize light by adding designed gain and loss to photonic crystals with chiral edge states. The light is localized at corners due to second-order NHSE, subject to particular symmetries in the gain and loss introduced to the lattice. Specifically, photonic corner skin modes due to bipolar second-order NHSE and multiple-corner skin modes are predicted in continuous systems. The resulting interesting localization behavior of light should be of experimental interest and may be used to enhance light-matter interactions. Compared with the better known first-order NHSE, our results clearly demonstrate that second-order NHSE can be engineered by use of crystal symmetries. Photonic crystals are hence identified as a versatile platform to investigate and exploit second-order NHSE.

*Note added*. Recently, we noticed four related studies posted on arXiv, including three theoretical studies [86–88] and one experimental study [89].


[1] S. Yao and Z. Wang, Edge States and Topological Invariants of Non-Hermitian Systems, Phys. Rev. Lett. **121**, 086803 (2018).

[2] C. H. Lee and R. Thomale, Anatomy of skin modes and topology in non-Hermitian systems, Phys. Rev. B **99**, 201103(R) (2019).

[3] N. Okuma, K. Kawabata, K. Shiozaki, and M. Sato, Topological Origin of Non-Hermitian Skin Effects, Phys. Rev. Lett. **124**, 086801 (2020).

[4] K. Zhang, Z. Yang, and C. Fang, Correspondence between Winding Numbers and Skin Modes in Non-Hermitian Systems, Phys. Rev. Lett. **125**, 126402 (2020).

[5] K. Kawabata, K. Shiozaki, M. Ueda, and M. Sato, Symmetry and Topology in Non-Hermitian Physics, Phys. Rev. X **9**, 041015 (2019).

[6] K. Yokomizo and S. Murakami, Non-Bloch Band Theory of Non-Hermitian Systems, Phys. Rev. Lett. **123**, 066404 (2019).

[7] Z. Yang, K. Zhang, C. Fang, and J. Hu, Non-Hermitian Bulk-Boundary Correspondence and Auxiliary Generalized Brillouin Zone Theory, Phys. Rev. Lett. **125**, 226402 (2020).

[8] T. S. Deng and W. Yi, Non-Bloch topological invariants in a non-Hermitian domain wall system, Phys. Rev. B **100**, 035102 (2019).

[9] L. Xiao, T. Deng, K. Wang, G. Zhu, Z. Wang, W. Yi, and P. Xue, Non-Hermitian bulk–boundary correspondence in quantum dynamics, Nat. Phys. **16**, 761 (2020).

[10] T. Helbig, T. Hofmann, S. Imhof, M. Abdelghany, T. Kiessling, L. W. Molenkamp, C. H. Lee, A. Szameit, M. Greiter, and R. Thomale, Generalized bulk–boundary correspondence in non-Hermitian topolectrical circuits, Nat. Phys. **16**, 747 (2020).

[11] T. Hofmann, T. Helbig, F. Schindler, N. Salgo, M. Brzezińska, M. Greiter, T. Kiessling, D. Wolf, A. Vollhardt, A. Kabaši, C. H. Lee, A. Bilušić, R. Thomale, and T. Neupert, Reciprocal skin effect and its realization in a topolectrical circuit, Phys. Rev. Res. **2**, 023265 (2020).

[12] C. H. Lee, L. Li, and J. Gong, Hybrid Higher-Order Skin-Topological Modes in Nonreciprocal Systems, Phys. Rev. Lett. **123**, 016805 (2019).

[13] L. Li, C. H. Lee, and J. Gong, Topological Switch for Non-Hermitian Skin Effect in Cold-Atom Systems with Loss, Phys. Rev. Lett. **124**, 250402 (2020).

[14] K. Kawabata, M. Sato, and K. Shiozaki, Higher-order non-Hermitian skin effect, Phys. Rev. B **102**, 205118 (2020).

[15] R. Okugawa, R. Takahashi, and K. Yokomizo, Second-order topological non-Hermitian skin effects, Phys. Rev. B **102**, 241202(R) (2020).

[16] Y. Fu, J. Hu, and S. Wan, Non-Hermitian second-order skin and topological modes, Phys. Rev. B **103**, 045420 (2021).

[17] K. M. Kim and M. J. Park, Disorder-driven phase transition in the second-order non-Hermitian skin effect, Phys. Rev. B **104**, L121101 (2021).

[18] L. S. Palacios, S. Tchoumakov, M. Guix, I. Pagonabarraga, S. Sánchez, and A. G. Grushin, Guided accumulation of active particles by topological design of a second-order skin effect, Nat. Commun. **12**, 4691 (2021).

[19] D. Zou, T. Chen, W. He, J. Bao, C. H. Lee, H. Sun, and X. Zhang, Observation of hybrid higher-order skin-topological effect in non-Hermitian topolectrical circuits, Nat. Commun. **12**, 1 (2021).

[20] X. Zhang, Y. Tian, J. H. Jiang, M. H. Lu, and Y. F. Chen, Observation of higher-order non-Hermitian skin effect, Nat. Commun. **12**, 5377 (2021).

[21] Sayed Ali Akbar Ghorashi, T. Li, and M. Sato, Non-Hermitian higher-order Weyl semimetals, Phys. Rev. B **104**, L161117 (2021).

[22] Sayed Ali Akbar Ghorashi, T. Li, M. Sato, and T. L. Hughes, Non-Hermitian higher-order Dirac semimetals, Phys. Rev. B **104**, L161116 (2021).

[23] C. Shang, S. Liu, R. Shao, P. Han, X. Zang, X. Zhang, K. N. Salama, W. Gao, C. H. Lee, R. Thomale, A. Manchon, S. Zhang, T. J. Cui, and U. Schwingenschlogl, Experimental identification of the second-order non-Hermitian skin effect with physics-graph-informed machine learning, Adv. Sci. **9**, 2202922 (2022).

[24] Y. Li, C. Liang, C. Wang, C. Lu, and Y.-C. Liu, Gain-Loss-Induced Hybrid Skin-Topological Effect, Phys. Rev. Lett. **128**, 223903 (2022).

[25] W. Zhu and J. Gong, Hybrid skin-topological modes without asymmetric couplings, Phys. Rev. B **106**, 035425 (2022).

[26] L. Lu, J. D. Joannopoulos, and M. Soljačić, Topological photonics, Nat. Photon. **8**, 821 (2014).

[27] A. B. Khanikaev and G. Shvets, Two-dimensional topological photonics, Nat. Photon. **11**, 763 (2017).

[28] B.-Y. Xie, H.-F. Wang, X.-Y. Zhu, M.-H. Lu, Z. D. Wang, and Y.-F. Chen, Photonics meets topology, Opt. Express **26**, 24531 (2018).

[29] T. Ozawa, H. M. Price, A. Amo, N. Goldman, M. Hafezi, L. Lu, M. C. Rechtsman, D. Schuster, J. Simon, O. Zilberberg, and I. Carusotto, Topological photonics, Rev. Mod. Phys. **91**, 015006 (2019).

[30] D. Smirnova, D. Leykam, Y. Chong, and Y. Kivshar, Nonlinear topological photonics, Appl. Phys. Rev. **7**, 021306 (2020).

[31] Y. Ota, K. Takata, T. Ozawa, A. Amo, Z. Jia, B. Kante, M. Notomi, Y. Arakawa, and S. Iwamoto, Active topological photonics, Nanophotonics **9**, 547 (2020).

[32] M. Kim, Z. Jacob, and J. Rho, Recent advances in 2D, 3D and higher-order topological photonics, Light: Sci. Appl. **9**, 1 (2020).

[33] L. Xie, L. Jin, and Z. Song, Antihelical edge states in two-dimensional photonic topological metals, Sci. Bull. **68**, 255 (2023).

[34] H. Xue, Y. Yang, and B. Zhang, Topological valley photonics: Physics and device applications, Adv. Photonics Res. **2**, 2100013 (2021).

[35] F. D. M. Haldane and S. Raghu, Possible Realization of Directional Optical Waveguides in Photonic Crystals with Broken Time-Reversal Symmetry, Phys. Rev. Lett. **100**, 013904 (2008).

[36] Z. Wang, Y. D. Chong, J. D. Joannopoulos, and M. Soljačić, Reflection-Free One-Way Edge Modes in a Gyromagnetic Photonic Crystal, Phys. Rev. Lett. **100**, 013905 (2008).

[37] Z. Wang, Y. Chong, J. D. Joannopoulos, and M. Soljačić, Observation of unidirectional backscattering-immune topological electromagnetic states, Nature (London) **461**, 772 (2009).

[38] M. C. Rechtsman, J. M. Zeuner, Y. Plotnik, Y. Lumer, D. Podolsky, F. Dreisow, S. Nolte, M. Segev, and A. Szameit, Photonic Floquet topological insulators, Nature (London) **496**, 196 (2013).

[39] L. Lu, Z. Wang, D. Ye, L. Ran, L. Fu, J. D. Joannopoulos, and M. Soljačić, Experimental observation of Weyl points, Science **349**, 622 (2015).

[40] R. El-Ganainy, K. G. Makris, M. Khajavikhan, Z. H. Musslimani, S. Rotter, and D. N. Christodoulides, Non-Hermitian physics and PT symmetry, Nat. Phys. **14**, 11 (2018).

[41] M. A. Miri and A. Alù, Exceptional points in optics and photonics, Science **363**, eaar7709 (2019).

[42] S. Malzard, C. Poli, and H. Schomerus, Topologically Protected Defect States in Open Photonic Systems with Non-Hermitian Charge-Conjugation and Parity-Time Symmetry, Phys. Rev. Lett. **115**, 200402 (2015).

[43] S. Weimann, M. Kremer, Y. Plotnik, Y. Lumer, S. Nolte, K. G. Makris, M. Segev, M. C. Rechtsman, and A. Szameit, Topologically protected bound states in photonic parity-time-symmetric crystals, Nat. Mater. **16**, 433 (2017).

[44] M. Pan, H. Zhao, P. Miao, S. Longhi, and L. Feng, Photonic zero mode in a non-Hermitian photonic lattice, Nat. Commun. **9**, 1308 (2018).

[45] K. Takata and M. Notomi, Photonic Topological Insulating Phase Induced Solely by Gain and Loss, Phys. Rev. Lett. **121**, 213902 (2018).

[46] X. W. Luo and C. Zhang, Higher-Order Topological Corner States Induced by Gain and Loss, Phys. Rev. Lett. **123**, 073601 (2019).

[47] Y. Ao, X. Hu, Y. You, C. Lu, Y. Fu, X. Wang, and Q. Gong, Topological Phase Transition in the Non-Hermitian Coupled Resonator Array, Phys. Rev. Lett. **125**, 013902 (2020).

[48] M. Parto, Y. G. Liu, B. Bahari, M. Khajavikhan, and D. N. Christodoulides, Non-Hermitian and topological photonics: Optics at an exceptional point, Nanophotonics **10**, 403 (2020).

[49] X. Zhou, J. Wu, and Y. Wu, Topological corner states in non-Hermitian photonic crystals, Opt. Commun. **466**, 125653 (2020).

[50] A. Y. Song, X. Q. Sun, A. Dutt, M. Minkov, C. Wojcik, H. Wang, I. A. D. Williamson, M. Orenstein, and S. Fan, $\mathcal{PT}$-Symmetric Topological Edge-Gain Effect, Phys. Rev. Lett. **125**, 033603 (2020).

[51] S. Xia, D. Kaltsas, D. Song, I. Komis, J. Xu, A. Szameit, H. Buljan, K. G. Makris, and Z. Chen, Nonlinear tuning of PT symmetry and non-Hermitian topological states, Science **372**, 72 (2021).

[52] J. Jiang, B. Yan, Y. Peng, J. Xie, A. Shi, and J. Liu, Multiband topological states in non-Hermitian photonic crystals, Opt. Lett. **47**, 437 (2022).

[53] H. Shen, B. Zhen, and L. Fu, Topological Band Theory for Non-Hermitian Hamiltonians, Phys. Rev. Lett. **120**, 146402 (2018).

[54] S. Yao, F. Song, and Z. Wang, Non-Hermitian Chern Bands, Phys. Rev. Lett. **121**, 136802 (2018).

[55] F. K. Kunst, E. Edvardsson, J. C. Budich, and E. J. Bergholtz, Biorthogonal Bulk-Boundary Correspondence in Non-Hermitian Systems, Phys. Rev. Lett. **121**, 026808 (2018).

[56] K. Kawabata, K. Shiozaki, and M. Ueda, Anomalous helical edge states in a non-Hermitian Chern insulator, Phys. Rev. B **98**, 165148 (2018).

[57] M. G. Silveirinha, Topological theory of non-Hermitian photonic systems, Phys. Rev. B **99**, 125155 (2019).

[58] M. Li, X. Ni, M. Weiner, A. Alù, and A. B. Khanikaev, Topological phases and nonreciprocal edge states in non-Hermitian Floquet insulators, Phys. Rev. B **100**, 045423 (2019).

[59] H. T. Teo, H. Xue, and B. Zhang, Topological phase transition induced by gain and loss in a photonic Chern insulator, Phys. Rev. A **105**, 053510 (2022).

[60] M. Hafezi, E. A. Demler, M. D. Lukin, and J. M. Taylor, Robust optical delay lines with topological protection, Nat. Phys. **7**, 907 (2011).

[61] H. Hodaei, A. U. Hassan, S. Wittek, H. Garcia-Gracia, R. El-Ganainy, D. N. Christodoulides, and M. Khajavikhan, Enhanced sensitivity at higher-order exceptional points, Nature (London) **548**, 187 (2017).

[62] C. Zeng, Y. Sun, G. Li, Y. Li, H. Jiang, Y. Yang, and H. Chen, Enhanced sensitivity at high-order exceptional points in a passive wireless sensing system, Opt. Express **27**, 27562 (2019).

[63] G. Harari, M. A. Bandres, Y. Lumer, M. C. Rechtsman, Y. D. Chong, M. Khajavikhan, D. N. Christodoulides, and M. Segev, Topological insulator laser: Theory, Science **359**, eaar4003 (2018).

[64] M. A. Bandres, S. Wittek, G. Harari, M. Parto, J. Ren, M. Segev, D. N. Christodoulides, and M. Khajavikhan, Topological insulator laser: Experiments, Science **359**, eaar4005 (2018).

[65] Y. Zeng, U. Chattopadhyay, B. Zhu, B. Qiang, J. Li, Y. Jin, L. Li, A. G. Davies, E. H. Linfield, B. Zhang, Y. Chong, and Q. J. Wang, Electrically pumped topological laser with valley edge modes, Nature (London) **578**, 246 (2020).

[66] B. Y. Xie, H. F. Wang, H. X. Wang, X. Y. Zhu, J. H. Jiang, M. H. Lu, and Y. F. Chen, Second-order photonic topological insulator with corner states, Phys. Rev. B **98**, 205147 (2018).

[67] J. Noh, W. A. Benalcazar, S. Huang, M. J. Collins, K. P. Chen, T. L. Hughes, and M. C. Rechtsman, Topological protection of photonic mid-gap defect modes, Nat. Photon. **12**, 408 (2018).

[68] X. D. Chen, W. M. Deng, F. L. Shi, F. L. Zhao, M. Chen, and J. W. Dong, Direct Observation of Corner States in Second-Order Topological Photonic Crystal Slabs, Phys. Rev. Lett. **122**, 233902 (2019).

[69] L. Zhang, Y. Yang, Z.-K. Lin, P. Qin, Q. Chen, F. Gao, E. Li, J.-H. Jiang, B. Zhang, H. Chen, L. Zhang, P. Qin, Q. Chen, F. Gao, E. Li, H. Chen, Y. Yang, B. Zhang, Z.-k. Lin, and J.-h. Jiang, Higher-order topological states in surface-wave photonic crystals, Adv. Sci. **7**, 1902724 (2020).

[70] X. Zhu, H. Wang, S. K. Gupta, H. Zhang, B. Xie, M. Lu, and Y. Chen, Photonic non-Hermitian skin effect and non-Bloch bulk-boundary correspondence, Phys. Rev. Res. **2**, 013280 (2020).

[71] Y. Song, W. Liu, L. Zheng, Y. Zhang, B. Wang, and P. Lu, Two-Dimensional Non-Hermitian Skin Effect in a Synthetic Photonic Lattice, Phys. Rev. Appl. **14**, 064076 (2020).

[72] S. Weidemann, M. Kremer, T. Helbig, T. Hofmann, A. Stegmaier, M. Greiter, R. Thomale, and A. Szameit, Topological funneling of light, Science **368**, 311 (2020).

[73] J. Zhong, K. Wang, Y. Park, V. Asadchy, C. C. Wojcik, A. Dutt, and S. Fan, Nontrivial point-gap topology and non-Hermitian skin effect in photonic crystals, Phys. Rev. B **104**, 125416 (2021).

[74] Q. Yan, H. Chen, and Y. Yang, Non-Hermitian skin effect and delocalized edge states in photonic crystals with anomalous parity-time symmetry, Prog. Electromagn. Res. **172**, 33 (2021).

[75] K. Yokomizo, T. Yoda, and S. Murakami, Non-Hermitian waves in a continuous periodic model and application to photonic crystals, Phys. Rev. Res. **4**, 023089 (2022).

[76] H. Gao, H. Xue, Z. Gu, L. Li, W. Zhu, Z. Su, J. Zhu, B. Zhang, and Y. D. Chong, Anomalous Floquet non-Hermitian skin effect in a ring resonator lattice, Phys. Rev. B **106**, 134112 (2022).

[77] H. Xin, W. Song, S. Wu, Z. Lin, S. Zhu, and T. Li, Manipulating the non-Hermitian skin effect in optical ring resonators, Phys. Rev. B **107**, 165401 (2023).

[78] F. Song, S. Yao, and Z. Wang, Non-Hermitian Topological Invariants in Real Space, Phys. Rev. Lett. **123**, 246801 (2019).

[79] K. Wang, A. Dutt, K. Y. Yang, C. C. Wojcik, J. Vučković, and S. Fan, Generating arbitrary topological windings of a non-Hermitian band, Science **371**, 1240 (2021).

[80] L. Zhang, Y. Yang, Y. Ge, Y. J. Guan, Q. Chen, Q. Yan, F. Chen, R. Xi, Y. Li, D. Jia, S. Q. Yuan, H. X. Sun, H. Chen, and B. Zhang, Acoustic non-Hermitian skin effect from twisted winding topology, Nat. Commun. **12**, 1 (2021).

[81] L. Li, W. X. Teo, S. Mu, and J. Gong, Direction reversal of non-Hermitian skin effect via coherent coupling, Phys. Rev. B **106**, 085427 (2022).

[82] Y. Poo, R. X. Wu, Z. Lin, Y. Yang, and C. T. Chan, Experimental Realization of Self-Guiding Unidirectional Electromagnetic Edge States, Phys. Rev. Lett. **106**, 093903 (2011).

[83] S. A. Skirlo, L. Lu, and M. Soljačić, Multimode One-Way Waveguides of Large Chern Numbers, Phys. Rev. Lett. **113**, 113904 (2014).

[84] G. G. Liu, P. Zhou, Y. Yang, H. Xue, X. Ren, X. Lin, H. xiang Sun, L. Bi, Y. Chong, and B. Zhang, Observation of an unpaired photonic Dirac point, Nat. Commun. **11**, 1873 (2020).

[85] H. X. Wang, G. Y. Guo, and J. H. Jiang, Band topology in classical waves: Wilson-loop approach to topological numbers and fragile topology, New J. Phys. **21**, 093029 (2019).

[86] X. Ma, K. Cao, X. Wang, Z. Wei, and S. Kou, Chiral Skin Effect, arXiv:2304.01422.

[87] F. Schindler, K. Gu, B. Lian, and K. Kawabata, Hermitian Bulk–Non-Hermitian Boundary Correspondence, arXiv:2304.03742.

[88] D. Nakamura, K. Inaka, N. Okuma, and M. Sato, Universal platform of point-gap topological phases from topological materials, arXiv:2304.08110.

[89] G.-G. Liu, S. Mandal, P. Zhou, X. Xi, R. Banerjee, Y.-H. Hu, M. Wei, M. Wang, Q. Wang, Z. Gao, H. Chen, Y. Yang, Y. Chong, and B. Zhang, Localization of chiral edge states by the non-Hermitian skin effect, arXiv:2305.13139.